STEM CELLS

Generation of vascularized retinal organoids containing microglia based on a PDMS microwell platform

Hang Chen[1]†, Yuqin Liang[2,3]†, Xihao Sun[2,3]†, Wei Xiong[4], Tingting Yang[5], Yuan Liang[1], Xiuhong Ye[1], Xiaoxue Li[3], Wenxuan Wang[6], Jianing Gu[3], Jun Zhang[7], Liqun Chen[8], Hon Fai Chan[9,10]*, Jiansu Chen[2,3,4]*

Retinal organoids (ROs) offer a biomimetic in vitro model for investigating human retinal development and disease. However, current ROs face several limitations, such as the absence of vascular networks and microglial cells (MGs). Here, we developed a vascularized retinal organoids (vROs) model by coculturing vascular organoids (VOs) with ROs in a V-bottom polydimethylsiloxane (PDMS) microwell platform. Through coculturing for 30 to 120 days, we observed the presence of tubular blood vessels at the center of vROs. Transcriptomic analysis revealed that the vascularization in ROs was associated with angiogenesis and immune response. Furthermore, we observed that MGs in VOs migrated and integrated into the vROs as VOs and ROs fused, with the vROs exhibiting responsiveness to inflammatory stimuli. The vROs expressed tight junction protein claudin-5 and displayed similar characteristics to the inner blood-retinal barrier (iBRB). These vRO models, which incorporate vascular structures and MGs, provide an alternate avenue for retinal vascular disease research and hold promise for future clinical applications.

INTRODUCTION

The research into human retinal development and disease mechanisms is hampered by challenges such as the limited availability of human retinal tissue (*1*). Current models used in retinal studies include animal models, two-dimensional (2D) monolayer cell culture, retinal explants, and retinal organoids (ROs) (*2*). However, animal models are limited by species differences between animals and humans (*3*, *4*), while the 2D monolayer cell culture lacks cell-cell and cell-matrix interactions present in 3D tissue (*5*). The emergence of ROs has provided a valuable in vitro model to overcome those limitations (*6*, *7*). These ROs exhibit remarkable structural, molecular, and functional similarities to the human retina (*8*, *9*). However, the lack of blood vessels and microglial cells (MGs) in ROs has limited their ability to faithfully recapitulate the complexity of in vivo organs (*10*). Therefore, the introduction of vascularization and MGs into ROs is essential for understanding retinal development and the pathogenesis of neurovascular diseases (*11*).

Neural organoids, such as ROs and brain organoids (BOs), derive from the ectoderm, whereas blood vessels develop from the mesoderm (*12*). The lack of blood vessels in ROs can be explained by the distinct embryonic origins of blood vessels and retinal tissue (*13*). Previously, attempts have been made to address this challenge by coculturing blood vessel cells and BOs. For instance, researchers established blood vessel networks in human BOs by embedding them in Matrigel mixed with endothelial cells (ECs) derived from the same induced pluripotent stem (iPS) cell source (*14*). Similarly, Shi and their team (*15*) developed a synchronous differentiation protocol to generate vascularized BOs by coculturing embryonic stem cells or iPS cells with human umbilical vein ECs (HUVECs). However, these vessels were simple endothelial tube structures without recapitulating the complex architecture of the vasculature, which consists of ECs, pericytes, and basement membrane components (*16*).

Recently, Wimmer *et al.* (*17*). successfully differentiated iPS cells into 3D human vascular organoids (VOs). These VOs comprise ECs and pericytes that can self-assemble into a functional capillary network. This in vitro blood vessel model provides a new model for blood vessel disease research and drug development (*18*). Furthermore, Sun *et al.* (*19*) and Kong *et al.* (*20*) developed vascularized BOs and cortical organoids (COs) by fusing BOs and COs with VOs. They discovered the presence of MGs in VOs and introduced MGs into BOs and COs. Recently, Inagaki *et al.* (*21*) used dissociated vascular cells derived from mature VOs and cocultured with iPS cells to generate vascularized ROs (vROs) in about 60 days. However, MGs were not observed in their vROs. They also embedded the VOs and ROs (day 30) in Matrigel and cocultured them in a 96-well U-bottom plate, but they failed to generate vROs. Therefore, obtaining vROs containing MGs may require referencing the strategy of developing vascularized BOs, the characteristics of RO development, and other technologies.

Usually, VOs were generated by human pluripotent stem cells (hPSCs) suspension culture, forming aggregates in low-attachment six-well plates (*17*). However, hPSCs exhibited heterogeneity in aggregate size in suspension culture differentiation (*22*). Recently, some researchers fused VOs with tissue organoids in parafilm, low-adhesion plates, or organoids on chip to generate vascularized organoids (*19*, *20*, *23*). In our approach, we applied a 26-well V-bottom polydimethylsiloxane (PDMS) microwell platform to generate VOs to reduce organoid heterogeneity. Subsequently, using the same

[1]Department of Ophthalmology, The First Affiliated Hospital of Jinan University, Guangzhou 510632, China. [2]Aier Eye Hospital, Jinan University, Guangzhou 510010, China. [3]Aier Academy of Ophthalmology, Central South University, Changsha 410015, China. [4]Key Laboratory for Regenerative Medicine, Ministry of Education, Jinan University, Guangzhou 510632, China. [5]Department of Ophthalmology, Affiliated Qingyuan Hospital, Guangzhou Medical University, Qingyuan People's Hospital, Qingyuan 511518, China. [6]Department of Ophthalmology, People's Hospital of Shenzhen Baoan District, Shenzhen 518101, China. [7]Department of Optoelectronic Engineering, College of Physics and Optoelectronic Engineering, Jinan University, Guangzhou 510632, China. [8]Academy of Medical Engineering and Translational Medicine, Medical College, Tianjin University, Tianjin 300072, China. [9]Institute for Tissue Engineering and Regenerative Medicine, The Chinese University of Hong Kong, Hong Kong SAR 999077, China. [10]Key Laboratory for Regenerative Medicine of the Ministry of Education of China, School of Biomedical Sciences, Faculty of Medicine, The Chinese University of Hong Kong, Shatin, Hong Kong SAR 999077, China.
*Corresponding author. Email: honfaichan@cuhk.edu.hk (H.F.C.); chenjiansu2000@163.com (J.C.)
†These author contributed equally to this work.

mold, we placed ROs above VOs for fusion. Our results showed that the V-bottom PDMS microwell is very effective in promoting the generation of vROs.

To construct vROs with biomimetic characteristics, we fused ROs and VOs in a V-bottom PDMS microwell. First, we generated ROs and VOs derived from iPS cells separately. After coculturing ROs and VOs for 30 to 120 days, we observed RO vascularization in vROs. Second, we unraveled the cellular molecular mechanism in vROs by transcriptomic analysis and validation assay. Third, we identified MGs in the VOs and vROs and explored the response of vROs containing MGs to lipopolysaccharide (LPS) stimulation. Last, we assessed the characteristics of the vROs, especially the structural features of the inner blood-retinal barrier (iBRB). This study demonstrated the generation of a vRO model containing vascular structures and MGs, which opens up new possibilities for disease modeling and drug discovery.

RESULTS

Generation and characterization of VOs

We generated VOs by modifying a previously established differentiation protocol (*17*). The preparation of the PDMS microwell platform and the differentiation process of the VOs are illustrated in Fig. 1A and fig. S1A. The coefficient variation (CV) of VOs diameters was measured at 7.322 ± 1.119 for 96-well V-bottom plates, 11.980 ± 2.770 for the PDMS microwell platform, and 39.650 ± 2.208 for six-well plates. Both the PDMS microwell platform and 96-well V-bottom plates demonstrated lower CV compared to the six-well plates, with a statistically significant difference observed between these groups ($P < 0.05$) (fig. S1B). There was no significant statistical difference found between the PDMS microwell platform and the 96-well V-bottom plates ($P > 0.05$) (fig. S1B). The V-bottom 96-well is approximately 11 mm deep and 8 mm wide, whereas the diameter of the PDMS microwell platform is 35 mm and consists of 26 V-bottom microwells, with each V-bottom microwell 3 mm in height and 2 mm in diameter. The depth of the 96-well makes it difficult for researchers to perform the fusion of organoids under a microscope (fig. S1C). To ensure consistent formation of vascular aggregates and generate vROs, iPS cells were seeded in the V-bottom PDMS microwell platform (about 1000 cells per microcavity) to facilitate cell spheroid formation (Fig. 1B). Under the stimulation by vascular endothelial growth factor–A (VEGF-A) and fibroblast growth factor–2 (FGF-2), we observed vascular sprouting and the gradual formation of vascular networks. Between days 12 and 15, the vascular networks were isolated from the gel and cultured in 96-well low-adhesion plates, allowing for self-assembly into VOs (Fig. 1B). To assess vascular development, we conducted a reverse transcription quantitative polymerase chain reaction (RT-qPCR) analysis of VOs at various time points. The results reveal a progressively increased expression of vascular-related genes such as *CD31*, *PDGF*β, and *CDH5* (Fig. 1C). Immunofluorescence staining showed that CD31-labeled blood vessel networks wrapped around by platelet-derived growth factor–β (PDGFβ)–labeled pericytes on VOs of day 25 (Fig. 1D). Furthermore, the quantitative vascular analysis tool (Angiotool) was used to evaluate vascular-related metrics (*24*). On day 25, the average vessel area was measured at 37.450 ± 5.490%, with an average vessel length of approximately 24.850 ± 7.881 mm and a mean Euclidean (*E*) lacunarity of 0.280 ± 0.096 (Fig. 1, E to G). We also generated VOs from iPS cells expressing green fluorescent protein (GFP; fig. S2A). Immunofluorescence staining showed that GFP-VOs contained CD31-labeled blood vessels, covered with PDGFβ-labeled pericytes and collagen IV (COL IV)–labeled basement membrane (Fig. 1, H and I). To evaluate ECs functionality within VOs, we assessed DiI-acetylated low-density lipoprotein (DiI-Ac-LDL) uptake following previous research (*25*). VOs on day 15 demonstrated efficient DiI-Ac-LDL uptake (Fig. 1J). In summary, we generated a fully structured VO model.

Establishment of vROs using a V-bottom PDMS microwell platform

In this study, we adopted a multistep strategy for generating vROs. First, we generated ROs and performed immunofluorescence staining on ROs at different developmental stages. Immunofluorescence staining revealed positive staining of retinal progenitor cell marker RX, neuroretinal markers PAX6 and CHX10, retinal ganglion cells marker BRN3A, amacrine cells marker AP2α, photoreceptor precursor cells marker OTX2, rod cells marker Rhodopsin, and cone cells marker M/L opsin (fig. S2, B and C). These results indicated the successful generation of ROs. To generate vROs, we used a V-bottom PDMS microwell platform to fuse ROs and VOs in a microwell (Fig. 2A). On day 5 of VO generation, VO was embedded in a 1:1 mixture of Matrigel and collagen I. Subsequently, RO at day 60 was added above the VO and cultured in a retinal maturation medium (RMM) containing VEGF-A (20 ng/ml; Fig. 2B). To verify whether the vROs exhibited blood vessel structures, we used CD31 as a marker to detect vROs vascularization. On days 30 and 60 of coculturing, we found the presence of CD31-positive tube-like blood vessel structures at the center of vROs (Fig. 2, C and D). We also detected neural retina labeled by CHX10, photoreceptor precursor cells labeled by CRX and OTX2, and amacrine cells labeled by AP2α (Fig. 2, C and D). In contrast, no blood vessel structures were observed in the ROs (Fig. 2C). In addition, we observed that the CD31-labeled endothelial-like tubes were covered by PDGFβ-labeled pericytes of vROs at 30 days of coculture (Fig. 2E). Notably, the vascular structures of vROs on day 30 of coculturing displayed a diameter of 6.36 ± 1.51 μm (Fig. 2F). Since photoreceptor cells are a crucial component of vROs, we also detected the presence of photoreceptor cells in late-stage vROs. Bright-field imaging revealed the presence of photoreceptor outer segment (OS) in vROs at day 180 (Fig. 3A). Immunofluorescence staining results indicated that both blood vessels and photoreceptor cells were observed in vROs at day 180 (Fig. 3B). In some cases, blood vessels were located in the deeper layer, while the rod cells and cone cells were located in the superficial layer, resembling the deep capillaries found in the human retina in vivo (Fig. 3C). Furthermore, confocal 3D imaging confirmed that blood vessels were located underneath the photoreceptor cells (Fig. 3, D and E). In summary, we constructed vROs that exhibited typical blood vessels and could be maintained in vitro for 120 days.

Transcriptomic analysis of vROs and ROs

To investigate the transcriptomic differences between ROs and vROs, we collected RNA from vROs cocultured for 30 days and RO samples and performed bulk RNA sequencing. The Principal components analysis showed obvious differences between the two groups (Fig. 4A). To identify differentially expressed genes (DEGs), we set the thresholds of $|\log_2(\text{fold change}) > 1|$ and Q value <0.05. We found 736 up-regulated genes and 102 down-regulated genes (Fig. 4B). Gene ontology (GO) analysis demonstrated that up-regulated DEGs were significantly enriched in biological processes

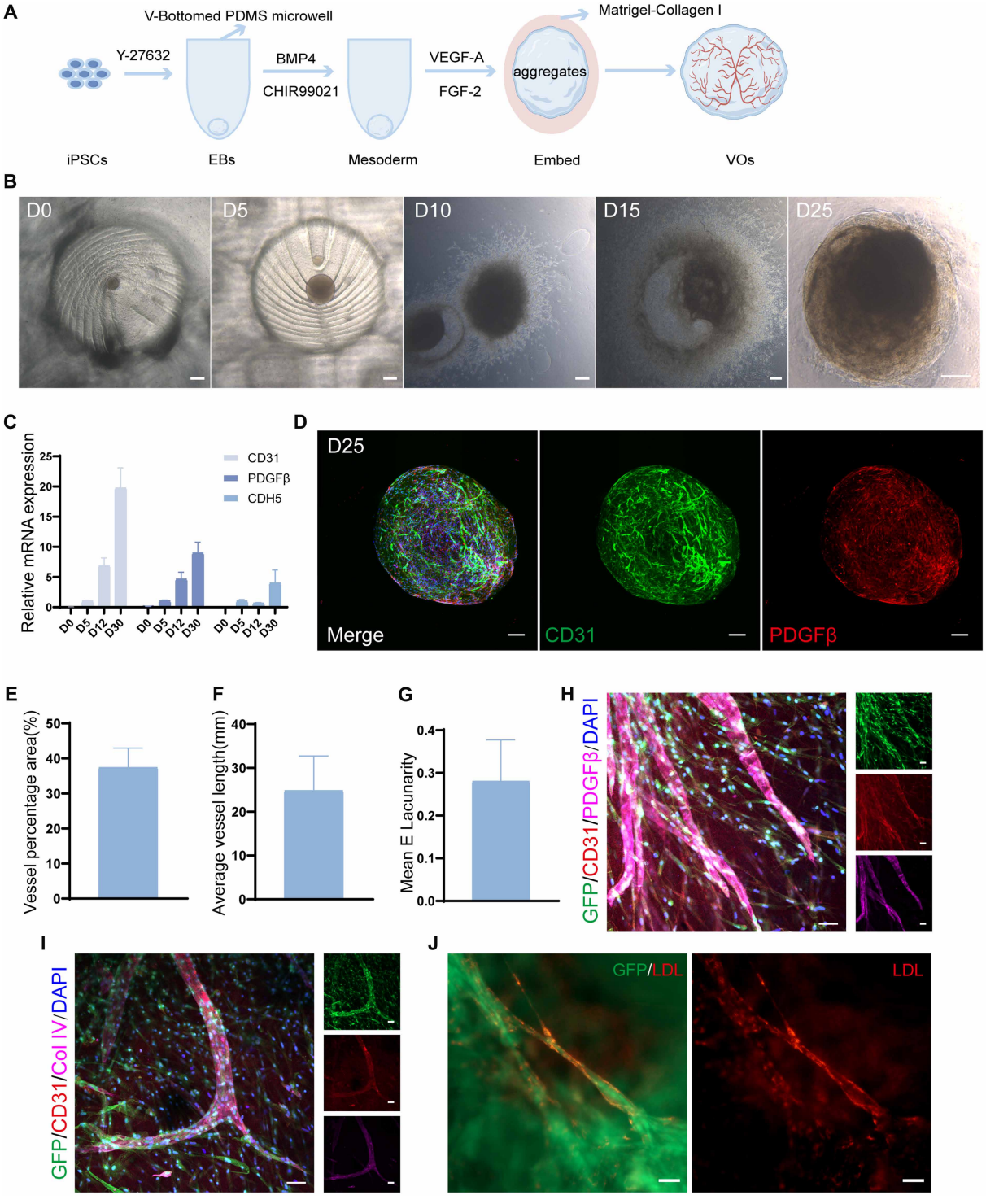

Fig. 1. Generation and characterization of VOs. (**A**) Schematic illustrating the process of generating VOs. (**B**) Bright-field images of VOs at various time points. Scale bars, 200 μm. (**C**) RT-qPCR analysis showed gene expression levels of vascular markers *CD31*, *PDGFβ*, and *CDH5* at days 0, 5, 12, and 30. (**D**) Immunofluorescence staining of CD31-positive blood vessels, PDGFβ-positive pericytes of VOs. Scale bars, 100 μm. (**E** to **G**) Results from Angiotool analysis of vascular networks at day 25 ($n = 14$ organoids). (**H** and **I**) Immunofluorescence staining of CD31-positive blood vessels, PDGFβ-positive pericytes, and COL IV–positive basement membrane in GFP-labeled VOs. Scale bars, 50 μm. (**J**) Living image of uptaking of DiI-Ac-LDL in VOs at day 15. Scale bars, 50 μm.

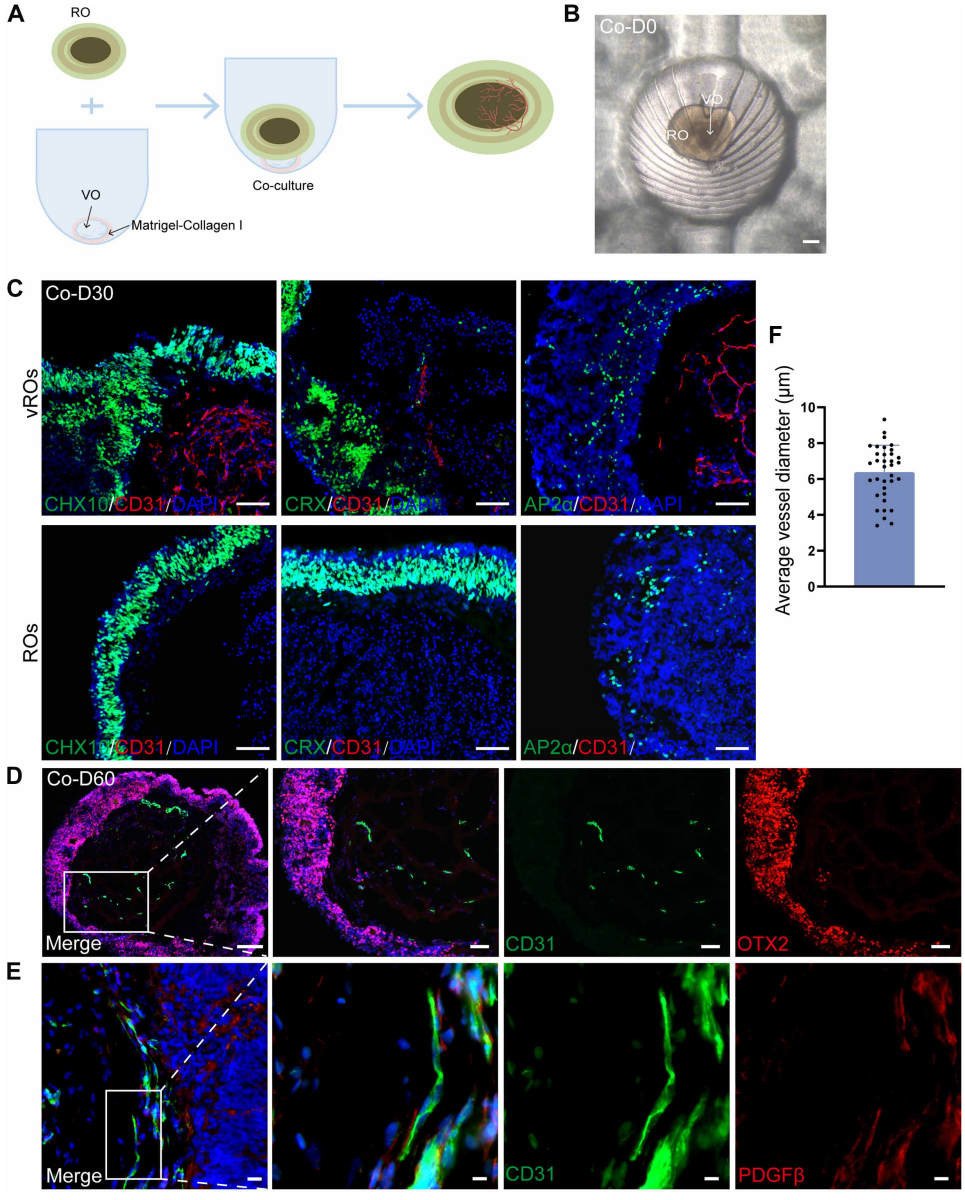

Fig. 2. Characterization of early coculture vROs. (**A**) Schematic illustrating the generation of vROs. (**B**) Bright-field images of coculture vROs at day 0. Scale bar, 200 μm. (**C**) At 30 days of coculture, immunofluorescence staining results of CD31-positive blood vessels, CHX10-positive neural retinal markers, CRX-positive photoreceptor precursor cells, and AP2α-positive amacrine cells. Scale bars, 50 μm. (**D**) At 60 days of coculture, immunofluorescence staining results of CD31-positive blood vessels and OTX2-positive photoreceptor precursor cells. Scale bars, (left) 100 μm and (right) 50 μm. (**E**) Immunofluorescence staining results of CD31-positive blood vessels and PDGFβ-positive pericytes of vROs at 30 days of coculture. Scale bars, (left) 20 μm and (right) 10 μm. (**F**) Vessel diameters of vROs at cocultured day 30 ($n = 10$ organoids, 2 to 4 vessels were measured per organoid).

(BP) related to angiogenesis, positive regulation of angiogenesis, and immune response (Fig. 4C). DEGs in the immune response, angiogenesis, and microglia were obtained from RNA sequencing data and presented in the form of heat maps (Fig. 4, D to F). The RT-qPCR validated that the expression levels of genes involved in immune response (*C1QC*, *CD22*, *TLR2*, *TLR4*, and *IRF8*), angiogenesis (*TIE1*, *ANGPT1*, *ANGPT2*, and *ECSCR*), and microglia (*AIF1*, *TMEM119*, *SPI1*, and *CSF1R*) were significantly higher in the vROs than the ROs ($P < 0.05$) (Fig. 4, G to I). Furthermore, we also found that the expression levels of genes associated with blood vessel (*CD31*, *PDGFβ*, and *CDH5*), retinal homeostasis (*DCN*, *HSD17B2*, and *PPARG*), retinal metabolic processes (*CYP1B1*, *ALDH1A3*, and *ALDH1A2*), and response to retinoic acid (RA) (*GATA6*, *GJA1*, *LRAT*, and *ADH1B*) were up-regulated in the vROs, which was consistent with transcriptomic data ($P < 0.05$) (fig. S3, A to E). These transcriptomic analyses and qPCR validation results suggested that vROs displayed angiogenesis and immune response signatures.

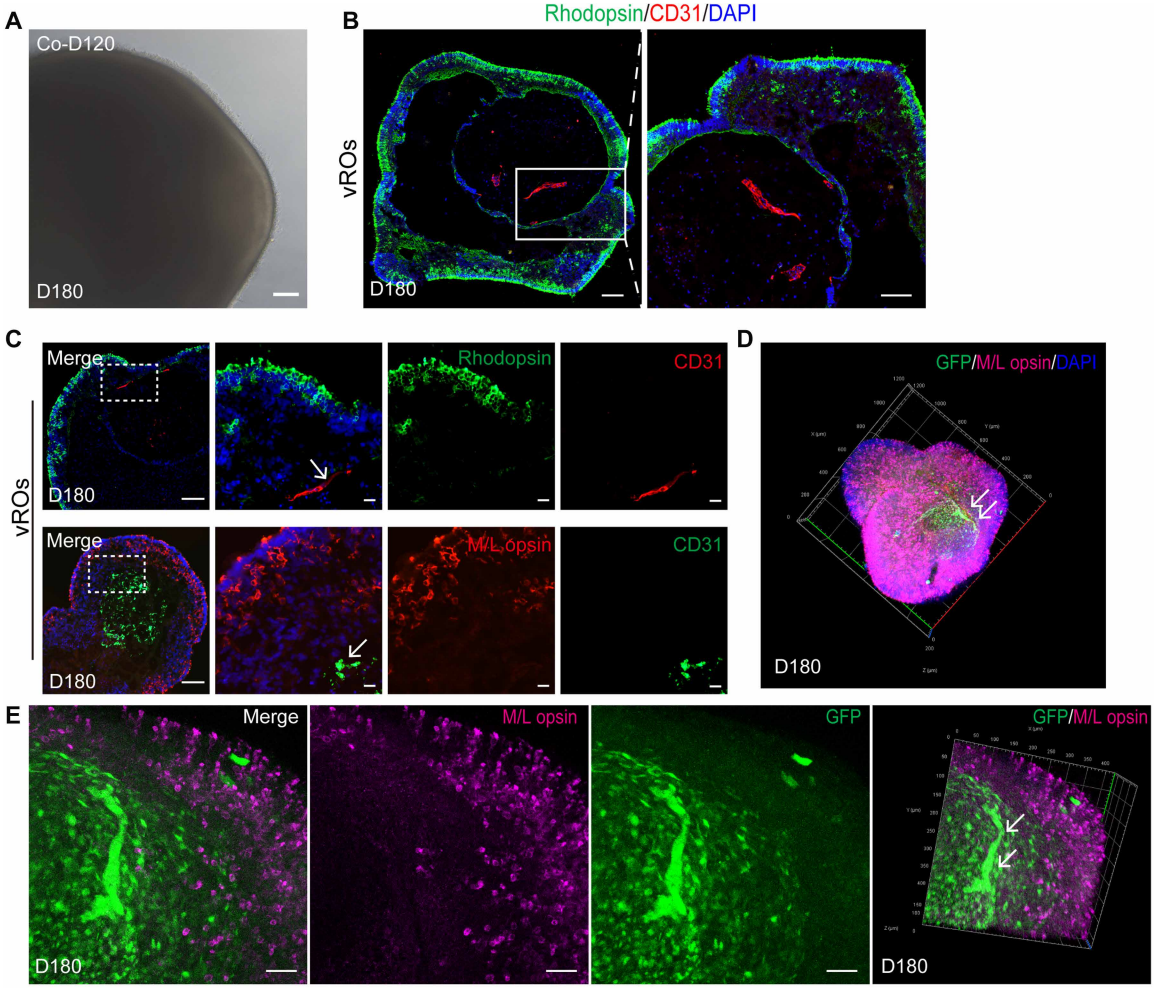

Fig. 3. Characterization of late coculture vROs. (**A**) Bright-field images of vROs at 180 days. Scale bar, 100 μm. (**B**) Immunofluorescence staining results of CD31-positive blood vessels and rhodopsin-positive rod cells. Scale bars, 100 μm. (**C**) Immunofluorescence staining results of CD31-positive blood vessels, Rhodopsin-positive rod cells, and M/L opsin–positive cone cells. Arrow: blood vessels. Scale bars, (left) 100 μm and (right) 20 μm. (**D** and **E**) Confocal 3D imaging of M/L opsin–positive cone cells in GFP-labeled vROs showed blood vessels inside the photoreceptor cells. Arrow, blood vessels. Scale bar, 50 μm.

Generation of VOs containing MGs

MGs originate from primitive macrophages in the mesoderm, which enter the central nervous system from the meninges during embryonic development and colonize within the retina (*26*). In our study, we observed that VOs contain MGs. We found that the expression of MG marker *AIF1* in VOs gradually increased over time (Fig. 5A). Furthermore, we found that about 86% IBA1-labeled MGs with an amoeboid morphology were located around the blood vessel, which is reminiscent of MGs surrounding retinal blood vessels in vivo (Fig. 5, B and C). To determine whether VEGF-A is required for MGs generation, we performed VOs cultures with and without VEGF-A. Immunofluorescence staining revealed that IBA1-positive MGs were detected in D15 VO cultured with or without VEGF-A (fig. S4A). The qPCR results showed that the expression level of MG-related gene *AIF1* was increased in the VOs treated with VEGF-A on day 15 compared with the control group, but there was no statistical difference between the two groups ($P > 0.05$) (fig. S4B). PLX5622, a colony-stimulating factor 1 receptor (CSF1R) inhibitor, has been shown to eliminate MGs (*27*). To further validate the identity of MGs, we treated VOs with 2 μM PLX5622 on day 23. After 7 days of treatment, most of the IBA1-labeled cells were absent compared to VOs treated with dimethyl sulfoxide (DMSO; Fig. 5D). The quantitative results of MGs showed that the amount of MGs in VOs + DMSO was $531.5 \pm 167.0/mm^2$ and that in VOs + PLX5622 was $22.15 \pm 7.984/mm^2$ ($P < 0.05$) (Fig. 5E). In addition, we treated VOs at day 27 with LPS (0.5 μg/ml) for 72 hours to induce an inflammatory response. The qPCR results showed that LPS stimulation caused a significant increase in the expression of the inflammatory cytokines *TNF*-α, *IL-8*, and MG marker *AIF1* ($P < 0.05$) (Fig. 5F). The expression levels of *TNF*-α and *IL-8* were reduced in PLX5622-treated VOs, suggesting that MGs in the VOs were involved in the LPS-induced immune response ($P < 0.05$) (Fig. 5F). These results confirmed the generation of MGs in VOs.

Generation of MGs in vROs that can respond to inflammatory stimuli

VOs immunofluorescence staining indicated the presence of MGs in VOs. Immunofluorescence staining showed that the blood vessels and

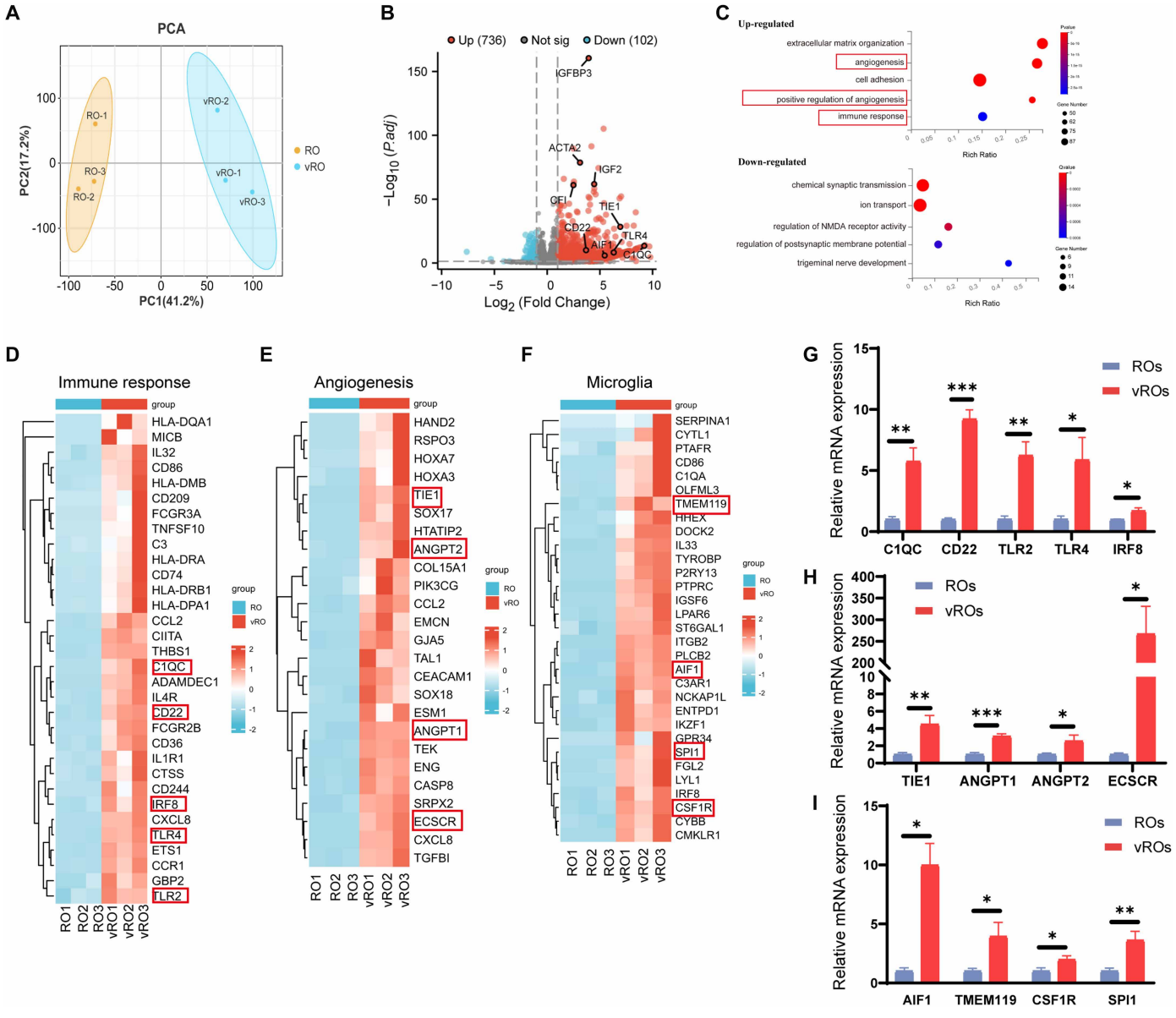

Fig. 4. Transcriptome characterization of vROs. (**A**) Principal components analysis diagram of the vRO groups and RO groups. (**B**) The volcano plots showed the DEGs between the vRO groups and the RO groups. (**C**) The top five up-regulated GO-enriched BPs and down-regulated GO-enriched BPs. (**D** to **F**) Heatmaps revealed DEGs associated with immune response, angiogenesis, and microglia. (**G** to **I**) RT-qPCR analysis showed the levels of genes related to immune response, angiogenesis, and microglia. Statistical method: unpaired two-tailed *t* tests. $^{*}P < 0.05$, $^{**}P < 0.01$, and $^{***}P < 0.001$.

MGs gradually migrated and integrated into the ROs as vROs generated (Fig. 6A and fig. S5A). To determine whether these MGs originated from VOs or ROs, we used immunofluorescence staining on vROs containing VOs derived from iPS cells expressing GFP. The results revealed IBA1-positive cells on the surface of vROs, while no IBA1-positive cells were found on the surface of ROs (Fig. 6B). Furthermore, about 96% of the GFP-positive cells were IBA1-labeled MGs in vROs (Fig. 6B and fig. S5B), indicating that the MGs in vROs originated from VOs. IBA1-positive MGs, as well as CHX10-labeled neuroretinal cells, OTX2-labeled photoreceptor precursor cells, and Rhodopsin-labeled rod cells, were detected in the cocultured vROs (Fig. 6C, and fig. S5, C and D). MGs attached to the surface of vROs and formed branches (Fig. 6C). This typical branching morphology suggested that they have further differentiated into resident-like MGs. In addition, there were blood vessels labeled with CD31 in the central region of vROs and GFP-positive MGs on the vROs (Fig. 6D). To investigate whether vROs containing MGs exhibit immune responses, we treated vROs and ROs with LPS (0.5 μg/ml) at day 90. Compared with ROs cultured alone, after 72 hours of stimulation, we found that the gene expression of cytokines was up-regulated, including pro-inflammatory markers such as *TNF*-α, *IL-8*, and anti-inflammatory markers *IL-10* and *IL-13* ($P < 0.05$) (Fig. 6E). Our results demonstrated that we have generated an in vitro vRO model containing both blood vessel structures and MGs and could respond to inflammatory stimuli.

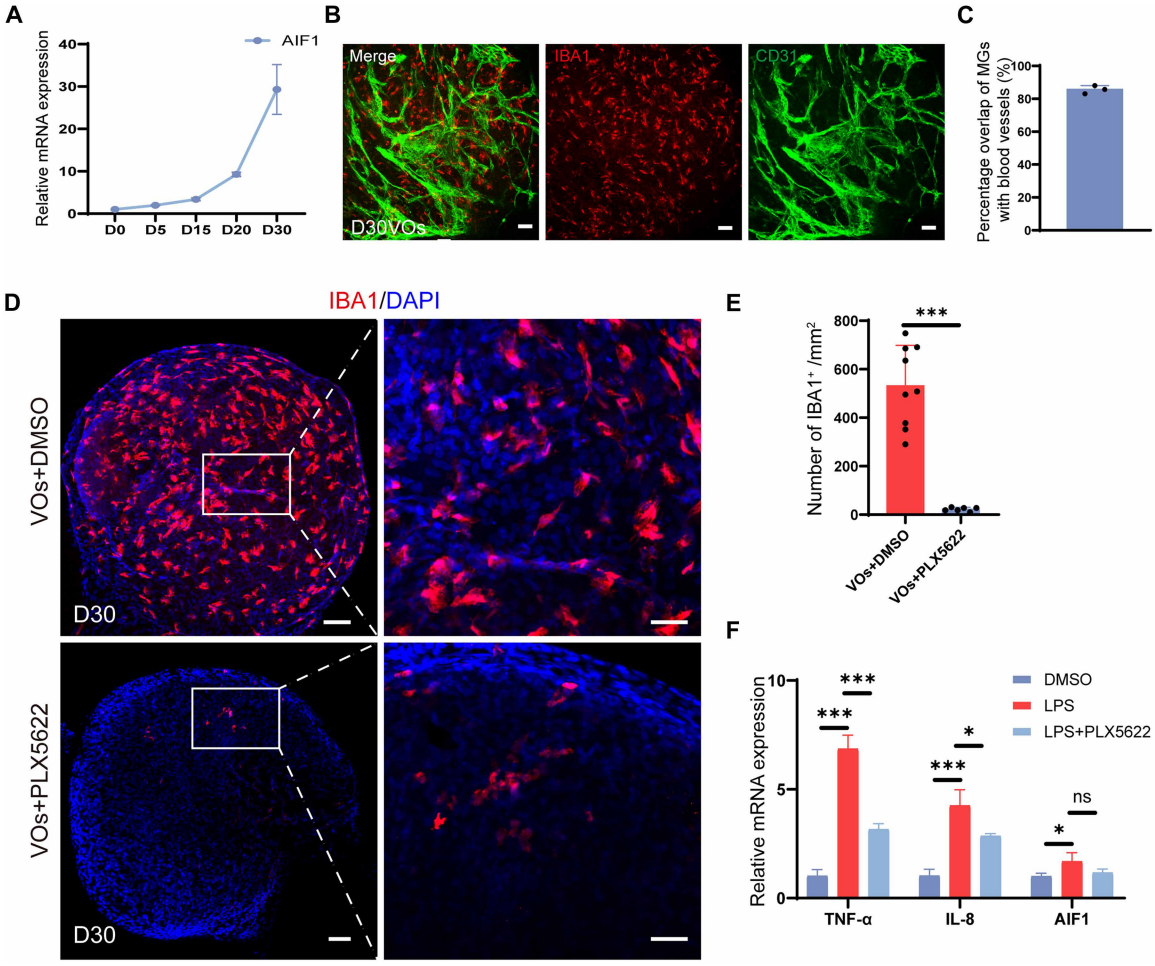

Fig. 5. Characterization of MGs in VOs. (**A**) RT-qPCR analysis showing the expression of MG-related gene *AIF1* at days 0, 5, 15, 20, and 30. (**B**) Immunofluorescence staining results of CD31-labeled blood vessels and IBA1-labeled MGs, Scale bars, 50 μm. (**C**) Percentage of overlap between MGs and blood vessels ($n = 3$ organoids). (**D**) Immunofluorescence staining results of IBA1-positive MGs in VOs with and without PLX5622 treatment for 7 days. Scale bars, (left) 100 μm and (right) 50 μm. (**E**) Quantification of the IBA1-positive cell number ($n = 6$ to 9 organoids). Statistical method: unpaired two-tailed *t* tests. ***$P < 0.001$. (**F**) RT-qPCR analysis of the gene expression of *TNF-α*, *IL-8*, and *AIF1* in VOs at day 30 treated with LPS (0.5 μg/ml) without or with PLX5622 treatment and using DMSO as a control. Statistical method: One-way ANOVA, ns indicates $P > 0.05$, *$P < 0.05$, and ***$P < 0.001$.

vROs exhibiting similar characteristics to iBRB

IBRB is essential for maintaining the homeostasis of the retinal microenvironment (*28*). The tight junctions between retinal microvascular ECs (RMECs) are a crucial characteristic of the iBRB. To further investigate whether our vROs exhibited structural features akin to those of the iBRB, we assessed the expression of tight junction protein claudin-5 and the endothelial window marker plasmalemma vesicle–associated protein (PLVAP). We found that in vROs at 30 days of coculture, CD31-labeled blood vessels expressed claudin-5 but did not express PLVAP (Fig. 7A). In contrast, ROs lacked claudin-5 expression (Fig. 7B). Further examination indicated that the blood vessels within VOs also expressed claudin-5 (Fig. 7C). Relative fluorescence density demonstrated that the expression of claudin-5 in VOs was lower than that in vROs ($P < 0.05$) (Fig. 7D). In addition, immunofluorescence staining results demonstrated that the CD31-labeled vascular structures in vROs at 30 days of coculture were surrounded by PDGFβ-labeled pericytes (Fig. 7E), while vascular structures were enveloped by IBA1-labeled MGs in vROs forming a neurovascular unit–like structure composed of ECs, pericytes, and MGs (Fig. 7, F and G). These structural features collectively suggested that the cellular composition and architecture of vROs exhibited similar characteristics to the iBRB in the human retina.

DISCUSSION

In recent years, the importance of constructing vascularized organoids for disease modeling and drug discovery has garnered increasing attention (*29*–*32*). Developing an appropriate in vitro model for the study of retinal vascular diseases remains a challenge (*10*, *13*). This study constructed vROs by generating VOs in a V-bottom PDMS microwell platform and then fusing them with ROs for coculture using the platform. Notably, we generated vROs that contained both blood vessel structures and MGs. Further research revealed that vROs exhibited an immune response in situ and similar characteristics to the iBRB of the human retina. Our vRO

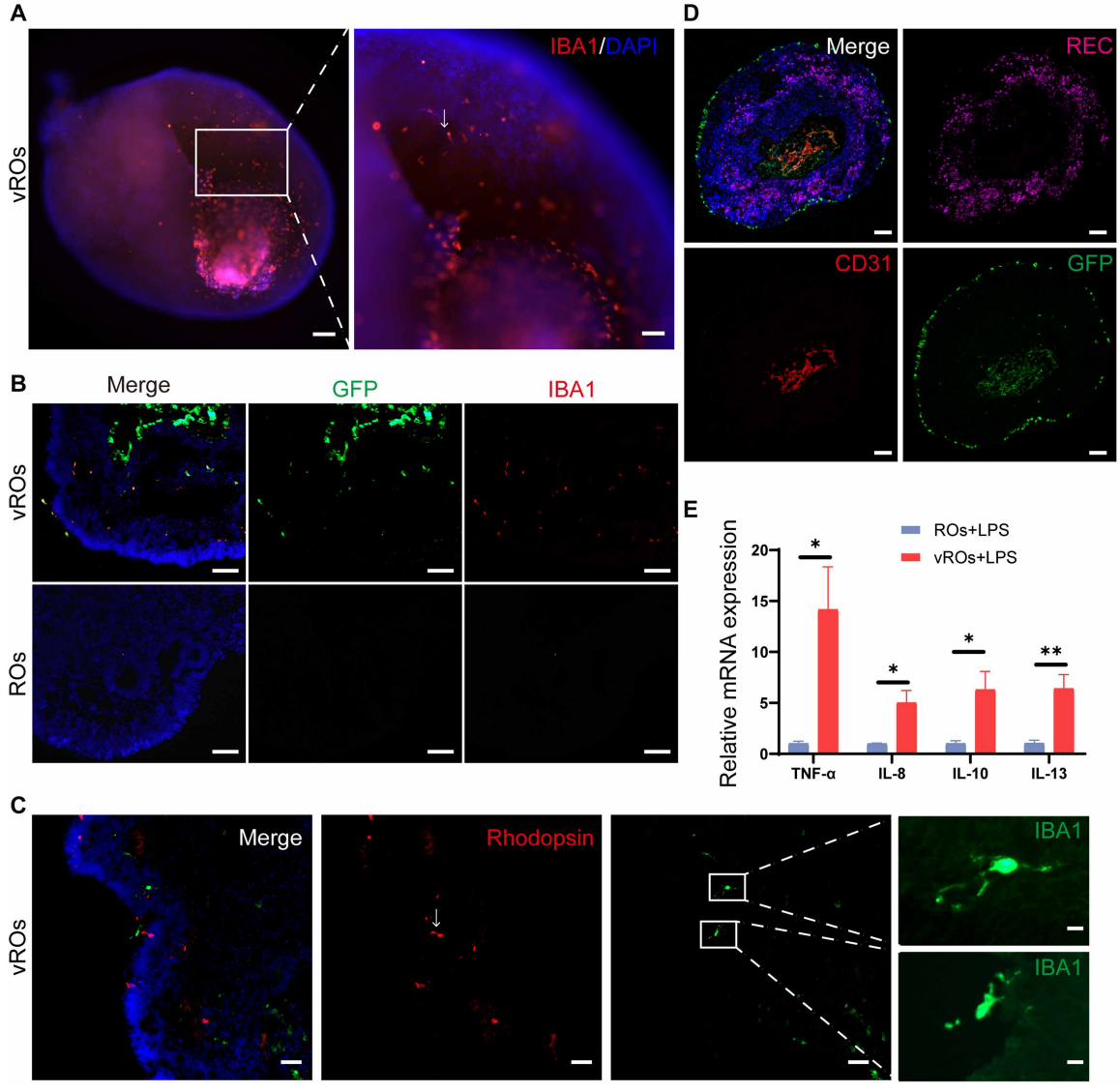

Fig. 6. An MGs-containing vRO model could respond to inflammatory triggers. (**A**) Whole-mount immunofluorescence staining results of IBA1-positive MGs in vROs. Scale bars, (left) 100 μm and (right) 50 μm. (**B**) Immunofluorescence staining results of IBA1-positive MGs colocalized with GFP-positive cells. Scale bars, 50 μm. (**C**) Immunofluorescence staining results of IBA1-positive MGs and rhodopsin-positive rod cells at 60 days of vROs. Arrow: rod cells. Scale bars, (left) 50 μm and (right) 5 μm. (**D**) Immunofluorescence staining results of GFP-positive cells, CD31-labeled blood vessels, and recoverin-positive photoreceptor precursor cells at coculture 40 days of vROs. REC, recoverin. Scale bars, 100 μm. (**E**) RT-qPCR analysis of the gene expression of *TNF-α*, *IL-8*, *IL-10*, and *IL-13* in vROs and ROs at day 90 treated with LPS (0.5 μg/ml). Statistical method: unpaired two-tailed *t* tests. $^{*}P < 0.05$ and $^{**}P < 0.01$.

model provides a new tool for retinal vascular disease research and clinical applications.

During the early incubation period, after fusing VOs with ROs for about 30 days, we observed CD31-labeled tubular blood vessel structures at the center of vROs. These blood vessel structures coexisted with neural retina cells and photoreceptor precursor cells. In contrast, ROs cultured in isolation showed a lack of vascular structures. The blood vessels' diameter was observed to fall within the typical range observed in human retinal capillaries (*33*). Therefore, our research confirmed that coculturing VOs with ROs resulted in the vascularization of ROs, consistent with findings for other vascularized BOs models (*19*, *20*, *34*, *35*). In vivo, ECs are the primary cell type in the inner layer of blood vessels, and pericytes are located outside the ECs and support and stabilize the vascular structures (*36*). Compared with previous studies of generating vascularized organoids by coculturing organoids with HUVECs or iPS cell–derived ECs (*37*, *38*), our study used VOs and detected CD31-labeled endothelial-like blood vessels covered by pericytes, which is consistent with findings reported previously (*19*, *20*).

It is well known that ROs induce the formation of mature photoreceptor cells at the late stage, which is a key feature of the functional retina (*39*). During the late stage of culture, ROs were observed to express photoreceptor OS. Previous studies reported that the cultivation time for vROs or vascularized BOs was approximately 60 days (*19*–*21*, *34*). However, in this study, even after 120 days of fusion and coculture of VOs and ROs, the vROs still contained rod

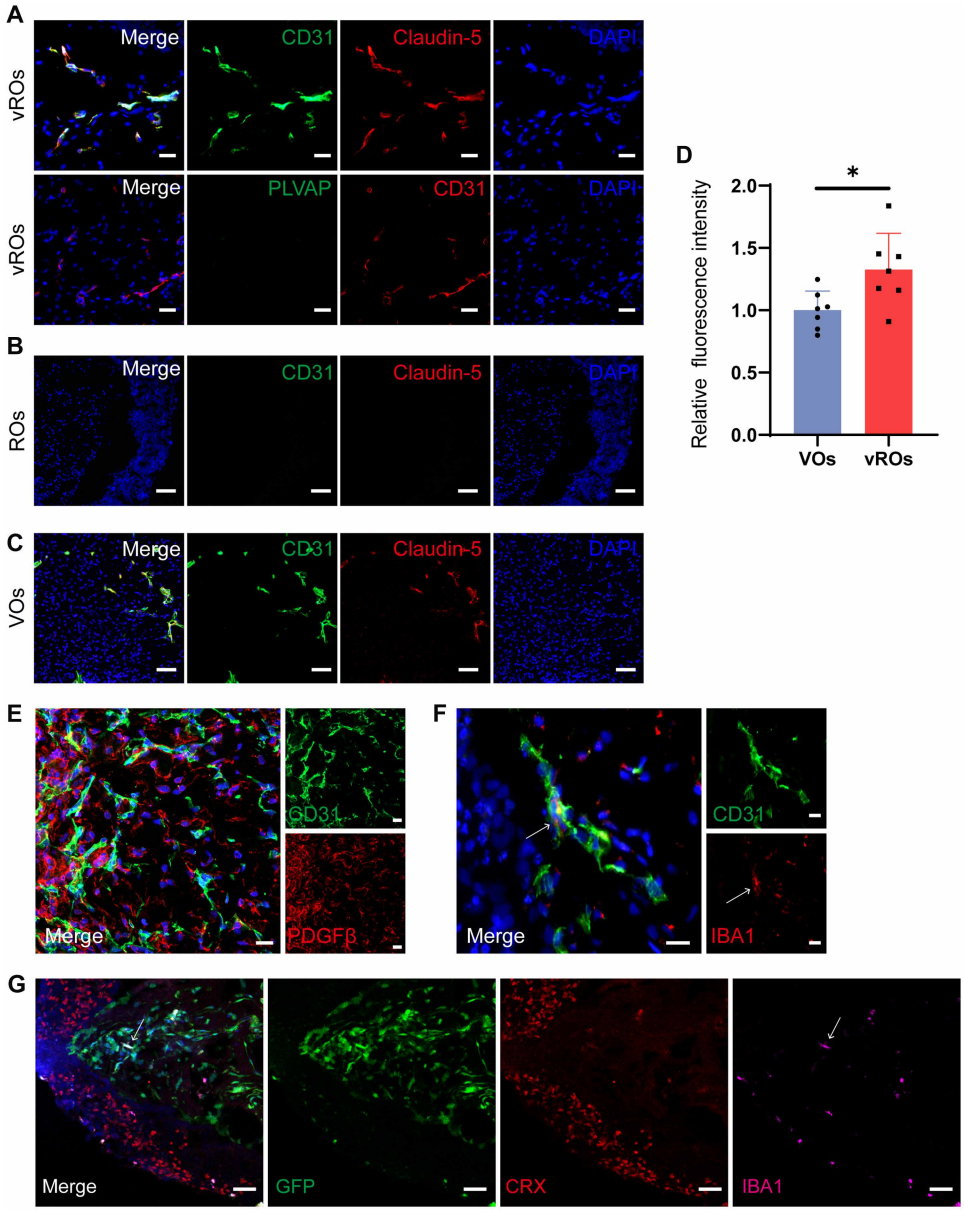

Fig. 7. vROs exhibited similar structural features to iBRB. (**A**) Immunofluorescence staining results of CD31, claudin-5, and PLVAP in vROs. Scale bars, 20 μm. (**B**) Immunofluorescence staining results of claudin-5 in ROs. Scale bars, 50 μm. (**C**) Immunofluorescence staining results of claudin-5 in VOs. Scale bars, 50 μm. (**D**) Relative fluorescence intensity of claudin-5 in VOs and vROs ($n = 7$ organoids). Statistical method: unpaired two-tailed t tests. $^*P < 0.05$. (**E**) Immunofluorescence staining results of CD31-positive blood vessels and PDGFβ-positive pericytes. Scale bars, 20 μm. (**F**) Immunofluorescence staining results showed colocalization of IBA1-labeled MGs with CD31-labeled blood vessels. Scale bars, 20 μm. (**G**) Immunofluorescence staining results showed colocalization of IBA1-labeled MGs, GFP-labeled blood vessels, and CRX-labeled photoreceptor precursor cells. Scale bars, 50 μm.

and cone cells and blood vessels, suggesting the long-term and stable culture of vascularized RO in vitro. We also observed that blood vessels in late-stage vROs were mostly located at the center of the vROs, similar to early-stage vROs. These results suggested that the vRO model could be highly valuable for the study of retinal vascular diseases in long-term culture.

Besides, IBA1-positive MG cells with amoeboid morphology were frequently found surrounding the blood vessels in VOs. MGs are resident immune cells in the human retina, playing crucial roles in synapse formation, remodeling, and vascular development (*40*). Sun *et al.* (*19*) observed that the MGs induced by VOs could respond to LPS stimulation and be inhibited by the PLX5622 reagent. Such findings were similar to the results of this study. The emergence of MGs was also inhibited by PLX5622, and MGs exhibited inflammatory responses to LPS stimulation. Costaining of markers of retinal development and MGs revealed interactions between MGs and retinal neural cells in the vROs. To determine the location of MGs, we used iPS cells expressing GFP to generate VOs before fusing VOs with ROs. Our results indicated that MGs were derived from VOs rather than ROs. Moreover, CD31-labeled tubular blood vessel

structures were identified at the center of the vROs. In contrast, conventional ROs typically lack both blood vessel structures and MG populations. Recently, Inagaki *et al.* (*21*) established a human vRO model by incorporating VO-derived ECs and pericytes in ROs, but MGs were absent. They also embedded the VOs and ROs (day 30) in Matrigel and cocultured them in a 96-well U-bottom plate. However, they failed to generate vROs. We attempted to use V-bottom 96-well plates for coculture and found that the depth of the 96-well makes it challenging to perform the fusion of organoids under a microscope. To overcome this, the V-bottom PDMS microwell platform was used to fuse VOs with ROs and generate vROs containing both blood vessels and MGs. Our study illuminated that an in vitro vRO model containing both blood vessels and MGs can facilitate research into MGs, retinal neurons, and vascular interactions, providing a more physiologically relevant platform for studying retinal development, disease pathology, and potential therapeutic interventions.

Recently, researchers found that organoids exhibited an immune response in situ after coculturing with iPS cell–derived MGs (*41*–*43*). Our transcriptome sequencing results indicated that DEGs of vROs were associated with the immune response BP. This is consistent with the results of Sabate *et al.* (*44*), which showed that the immune response BP was enhanced in midbrain organoids cocultured with iPS cell–derived MGs. Furthermore, we found that the gene expression levels of pro-inflammatory cytokines, such as *TNF*-α and *IL-8*, were significantly up-regulated in vROs compared to ROs alone following LPS treatment. An increase in the gene expression levels of anti-inflammatory cytokines, including *IL-10* and *IL-13*, was also observed. Chichagova *et al.* (*43*) have previously shown that both pro-inflammatory and anti-inflammatory cytokines were significantly up-regulated in ROs cocultured with MGs in response to LPS stimulation. Therefore, our results suggested that vROs containing MGs were immune-active and could serve as an in vitro model of functional retinas with immunocompetence.

The blood vessels in the inner retina have a continuous endothelium with a barrier function (*45*). Claudin-5 is one of the notable molecular markers of iBRB and the blood-brain barrier (BBB) (*46*). We observed that vROs expressed claudin-5, consistent with findings from previous studies (*19*, *29*, *34*). In contrast, we detected the absence of PLVAP, which is widely expressed in capillary and venous vessels but not in the BRB and BBB (*47*). In addition, the fluorescence intensity of claudin-5 in vROs was higher than that in VOs, indicating enhanced formation of tight junctions following the coculture of VOs with ROs. The neurovascular unit, consisting of CD31-labeled tubular blood vessel structures, pericytes, and MGs, was also detected in vROs (*48*), which is consistent with the findings of vascularized BOs (*19*). Our results suggested that vROs exhibited structural features similar to those of iBRB, which can provide a new avenue for in vitro studies of the retinal barrier.

In summary, we generated vROs containing both blood vessels and MGs via the V-bottom PDMS microwell. Moreover, we generated vROs with the structure of the iBRB. The vascular structures enveloped by IBA1-labeled MGs in vROs formed a neurovascular unit–like structure composed of ECs, pericytes, and MGs. Last, we successfully generated vROs with the structure of photoreceptor cells and blood vessels after long-term culture. These suggested that we could generate mature vROs via the V-bottom PDMS microwell platform.

Despite the above-mentioned advantages of our vROs, there are still some limitations that need to be addressed. For example, the detailed molecular mechanisms involving retinal development and vascularization of ROs remain to be uncovered. In addition, advanced chip design and fabrication for perfusion culture of vROs will be the focus of our next study. Moreover, we will explore the therapeutic potential of vROs for retinal transplantation for the treatment of retinal diseases.

MATERIALS AND METHODS

Preparation of V-bottom PDMS microwell platform

In our previous research, we successfully generated a V-bottom PDMS microwell platform via 3D printing (*49*). In this study, we developed a modified version of the 26-well V-bottom PDMS microwell platform. A mixture of 10 parts base material and 1 part curing agent (DowCorning, United States) was prepared and subjected to agitation in a magnetic stirrer at 500 RPM for 20 min to ensure adequate mixing. After mixing, the mixture was placed in a vacuum dryer to eliminate air bubbles. Next, the 3D-printed positive mold was positioned within a six-well plate, and 5 ml of the PDMS prepolymer was added. The six-well plate was then placed in an oven set at 70°C for 3 to 5 hours to ensure complete hardening of the PDMS microwell platform. Afterward, the PDMS microwell was carefully detached from the 3D-printed positive mold, and the PDMS microwell was autoclaved at 121°C for 30 min before being placed back into the six-well plate.

Maintenance of human iPS cells

We used three independent iPS cell lines in our experiments. Two blood-derived iPS cell lines were reported in our previous research (*49*). GFP-iPS cell line (CA4020106) was purchased from Cellapy Biotechnology (Beijing, China). In brief, iPS cells were maintained in mTeSR Plus medium (STEMCELL Technologies) in six-well plates (Corning, USA) coated with Matrigel (Corning, USA) at 37°C in 5% CO_2 in a humidified incubator. When iPS cells were approximately 85% confluent, they were passaged using 0.5 mM EDTA (Cellapy Biotechnology, Beijing, China) at split ratios from 1:8 to 1:10.

Generation of human VOs

VOs were differentiated following the method established by Wimmer *et al.* (*17*) with some modifications. iPS cells were dissociated into single cells using Accutase (STEMCELL Technologies). Then, the dissociated cells were resuspended in mTeSR Plus medium supplemented with 50 μM Y27632 and seeded into a V-bottom PDMS microwell platform. The plates were centrifuged at 50*g* for 8 min to form cell spheroids. On day 0, the medium was replaced with N2B27 medium containing BMP4 (30 ng/ml; MCE, HY-P7007) and 12 μM CHIR99021 (MCE, HY-10182). On day 3, the medium was replaced with N2B27 medium supplemented with VEGF-A (100 ng/ml; Peprotech 100-20) and 2 μM forskolin (Peprotech 6652995). On day 5, vascular aggregates were embedded in a 1:1 mixture of Matrigel:collagen I (Guangzhou Trauer Biotechnology, China). The aggregates were then cultured in a vascular endothelial cell medium (Sciencell) containing 15% fetal bovine serum (FBS; Gibco), VEGF-A (100 ng/ml), and FGF-2 (100 ng/ml; Peprotech 100-18B). The medium was changed every 48 hours. In addition, we also applied low-attachment V-bottom 96-well plates and six-well plates to generate VOs as compared study based on the above method.

Generation of ROs

Differentiation of ROs was performed as previously described with some modifications (*50*). On day 0, iPS cells were dissociated into

single cells using Accutase and suspended in a T25 bottle containing 20 μM Y27632 in mTeSR Plus medium. On days 1 to 3, to induce embryoid body (EB) formation, aggregates were cultured in a mixture of mTeSR Plus and neural induction medium (NIM) containing Dulbecco's modified Eagle's medium (DMEM)/F12 (Gibco), 1% N_2 supplement (Thermo Fisher Scientific, 17502048) and 1% nonessential amino acids (NEAA; Thermo Fisher Scientific, 11140035), heparin (2 μg/ml; STEMCELL Technologies), and the medium was changed at 3:1, 1:1, and 1:3 ratios of mTeSR Plus medium and NIM. On day 4, the medium comprised NIM only. On day 6, EBs were inoculated in Matrigel-coated 60-mm dishes and incubated with NIM until day 13, with the medium changed every other day. On day 14, the medium was changed to retinal differentiation medium containing DMEM/F12 (3:1), 2% B27 supplement (Thermo Fisher Scientific, 17504044), 1% NEAA, 1% GlutaMAX (Gibco), and penicillin/streptomycin (Gibco). Between days 25 and 28, neuroretinal domains showing the appearance of gold rings were isolated using a 10-μl pipette tip, and these isolated domains were self-organized into 3D ROs. On day 42, the medium was replaced with RMM containing DMEM/F12 (3:1), 10% FBS (Gibco), 2% B27 supplement, 1% GlutaMAX, 1% NEAA, 100 mM taurine (Sigma-Aldrich), 1 μM RA (Sigma-Aldrich), and penicillin/streptomycin. On day 90, the components of the RMM were changed to include DMEM/F12 (1:1), 10% FBS (Gibco), 1% N_2 supplement, 1% GlutaMAX, 1% NEAA, 100 mM taurine, 0.5 μM RA, and penicillin/streptomycin. On day 120, the RA was removed, after which the retinal organoids were cultured for an extended period.

Generation of vROs

To generate vROs, we fused VOs and ROs in a microwell of the 26-well V-bottom PDMS microwell platform. On day 5 of VO formation, the VO was embedded in a 1:1 mixture of Matrigel:collagen I. Then, RO at day 60 was positioned above the VO. Under a microscope, the positioning of the ROs relative to the VO was carefully adjusted to position the VOs beneath the ROs. After coculturing for 1 week, ROs and VOs gradually fused before they were transferred to low-adhesion 24-well plates for long-term incubation. During the coculture period, we used a coculture medium [RMM containing VEGF-A (20 ng/ml)]. The coculture medium was changed every 2 to 3 days. Following 2 months of coculture, the medium was switched to a VEGF-free RMM.

LDL-uptake assay

VOs on day 15 were washed three times with phosphate-buffered saline (PBS). Subsequently, VOs were incubated with Dil-Ac-LDL (10 μg/ml; Yiyuan Biotechnology, YB-0013) in vascular endothelial medium for 4 hours at 37°C. After incubation, the VOs were washed three times with vascular endothelial medium and then photographed using a Zeiss microscope.

Immunofluorescence

Organoids sectioned slices were fixed in 4% paraformaldehyde (PFA) at room temperature for 30 min, followed by three washes with PBS. They were then incubated in 0.1% Triton X-100 in PBS for 10 min and blocked with 3% bovine serum albumin in PBS for 1 hour at room temperature. The samples were subsequently incubated with the primary antibody overnight at 4°C. After being washed three times with PBS, they were stained with an Alexa Fluor–conjugated secondary antibody (Thermo Fisher Scientific, 1:1000) for 1 hour at room temperature. Following washes with PBS, they were stained with 4′,6-diamidino-2-phenylindole (DAPI; Solarbio C0060) (1 μg/ml) for 5 min. They were photographed and analyzed using a Zeiss microscope or Zeiss confocal microscope.

For whole-mount staining, the organoids were similarly fixed in 4% PFA for 30 min at room temperature and washed three times with PBS. They were treated with a permeabilization-blocking solution for 2 hours at room temperature; the composition of this solution was reported in previous studies (*17*). Following this step, the organoids were incubated with the primary antibody at 4°C for over 18 hours and then incubated for 1 hour at room temperature. After being washed three times with PBS with Tween 20 (PBST), they were stained with an Alexa Fluor–conjugated secondary antibody (Thermo Fisher Scientific, 1:1000) at room temperature for 2 hours and incubated with DAPI for 1 hour. After three final washes with PBST, the organoids were photographed and analyzed using a Zeiss microscope or Zeiss confocal microscope. Details about the primary antibodies can be found in Table S1.

Reverse transcription and quantitative polymerase chain reaction

Total RNA was extracted using the Total RNA Extraction Kit (Promega) and dissolved in ribonuclease-free water. The RNA samples were quantified by measuring the optical density (OD) value at 260 nm, and the OD 260/280 ratios for all RNA samples fell within the range of 1.8 to 2.1. The RNA reverse transcription was performed using HiScript II Q RT SuperMix (Vazyme), following the manufacturer's guidelines. Primer pairs were synthesized by Sangon Biotech (China). RT-qPCR was performed with the SYBR qPCR Master Mix (Vazyme) on a Roche LightCycler. The results of all samples were normalized to the housekeeping gene glyceraldehyde 3-phosphate dehydrogenase. The relative gene expression was calculated using the $2^{-\Delta\Delta Ct}$ method. All primer sequences used in the qPCR are provided in table S2.

RNA-sequencing analysis

vROs and ROs cultured with coculture medium at day 90 were suspended in 1 ml of TRIzol and stored at −80°C. Samples were divided into RO and vRO groups, with three biological replicates per group. RNA extraction, library construction, and RNA sequencing were conducted by BGI Tech Solutions Co. Ltd. (Shenzhen, China) on the BGISEQ platform, using paired-end sequencing with a length of 150. Following the filtration of raw data, clean reads were generated and aligned with the human genome assembly. The qualified reads were then normalized and quantified using transcripts per kilobase million values. DEGs between the two groups were screened by significance defined by $|\log_2(\text{fold change})| > 1$ and Q value <0.05. Further analysis was conducted through GO term enrichment and Kyoto Encyclopedia of Genes and Genomes enrichment analysis.

Statistical analysis

The data are presented as means ± SD. The number of replicates is indicated in the figure legends. GraphPad Prism 8.0 (GraphPad Software, San Diego, CA, USA) and FIJI version 1.49 software (National Institutes of Health, Bethesda, MD, USA) were used for data analysis. Statistical significance of the data was analyzed by an unpaired two-tailed t test for comparisons between two groups. One-way analysis of variance (ANOVA) was used to determine the differences among

the three groups. $P < 0.05$ was considered statistically significant. ns indicates $P > 0.05$, $^{*}P < 0.05$, $^{**}P < 0.01$, and $^{***}P < 0.001$.

Supplementary Materials

This PDF file includes:

Figs. S1 to S5

Tables S1 and S2

REFERENCES AND NOTES

1. C. A. Artero, J. F. Rodriguez, P. Jendelova, S. Erceg, Deciphering retinal diseases through the generation of three dimensional stem cell-derived organoids: Concise review. *Stem Cells* **37**, 1496–1504 (2019).
2. S. Schnichels, F. Paquet-Durand, M. Loscher, T. Tsai, J. Hurst, S. C. Joachim, A. Klettner, Retina in a dish: Cell cultures, retinal explants and animal models for common diseases of the retina. *Prog. Retin. Eye Res.* **81**, 100880 (2021).
3. R. W. Slijkerman, F. Song, G. D. Astuti, M. A. Huynen, E. van Wijk, K. Stieger, R. W. Collin, The pros and cons of vertebrate animal models for functional and therapeutic research on inherited retinal dystrophies. *Prog. Retin. Eye Res.* **48**, 137–159 (2015).
4. C. Kostic, Y. Arsenijevic, Animal modelling for inherited central vision loss. *J. Pathol.* **238**, 300–310 (2016).
5. X. Y. Tang, S. Wu, D. Wang, C. Chu, Y. Hong, M. Tao, H. Hu, M. Xu, X. Guo, Y. Liu, Human organoids in basic research and clinical applications. *Signal Transduct. Target. Ther.* **7**, 168 (2022).
6. M. Eiraku, N. Takata, H. Ishibashi, M. Kawada, E. Sakakura, S. Okuda, K. Sekiguchi, T. Adachi, Y. Sasai, Self-organizing optic-cup morphogenesis in three-dimensional culture. *Nature* **472**, 51–56 (2011).
7. T. Nakano, S. Ando, N. Takata, M. Kawada, K. Muguruma, K. Sekiguchi, K. Saito, S. Yonemura, M. Eiraku, Y. Sasai, Self-formation of optic cups and storable stratified neural retina from human ESCs. *Cell Stem Cell* **10**, 771–785 (2012).
8. A. Sridhar, A. Hoshino, C. R. Finkbeiner, A. Chitsazan, L. Dai, A. K. Haugan, K. M. Eschenbacher, D. L. Jackson, C. Trapnell, O. Bermingham-Mcdonogh, I. Glass, T. A. Reh, Single-cell transcriptomic comparison of human fetal retina, hPSC-derived retinal organoids, and long-term retinal cultures. *Cell Reports* **30**, 1644–1659.e4 (2020).
9. C. S. Cowan, M. Renner, M. De Gennaro, B. Gross-Scherf, D. Goldblum, Y. Hou, M. Munz, T. M. Rodrigues, J. Krol, T. Szikra, R. Cuttat, A. Waldt, P. Papasaikas, R. Diggelmann, C. P. Patino-Alvarez, P. Galliker, S. E. Spirig, D. Pavlinic, N. Gerber-Hollbach, S. Schuierer, A. Srdanovic, M. Balogh, R. Panero, A. Kusnyerik, A. Szabo, M. B. Stadler, S. Orgul, S. Picelli, P. W. Hasler, A. Hierlemann, H. Scholl, G. Roma, F. Nigsch, B. Roska, Cell types of the human retina and its organoids at single-cell resolution. *Cell* **182**, 1623–1640.e34 (2020).
10. K. Achberger, J. C. Haderspeck, A. Kleger, S. Liebau, Stem cell-based retina models. *Adv. Drug Deliv. Rev.* **140**, 33–50 (2019).
11. H. A. Strobel, S. M. Moss, J. B. Hoying, Vascularized tissue organoids. *Bioengineering* **10**, 124 (2023).
12. V. L. Bautch, K. M. Caron, Blood and lymphatic vessel formation. *Cold Spring Harbor Perspect. Biol.* **7**, a008268 (2015).
13. M. Li, L. Gao, L. Zhao, T. Zou, H. Xu, Toward the next generation of vascularized human neural organoids. *Med. Res. Rev.* **43**, 31–54 (2023).
14. M. T. Pham, K. M. Pollock, M. D. Rose, W. A. Cary, H. R. Stewart, P. Zhou, J. A. Nolta, B. Waldau, Generation of human vascularized brain organoids. *Neuroreport* **29**, 588–593 (2018).
15. Y. Shi, L. Sun, M. Wang, J. Liu, S. Zhong, R. Li, P. Li, L. Guo, A. Fang, R. Chen, W. P. Ge, Q. Wu, X. Wang, Vascularized human cortical organoids (vOrganoids) model cortical development in vivo. *PLOS. Biol.* **18**, e3000705 (2020).
16. P. Worsdorfer, N. Dalda, A. Kern, S. Kruger, N. Wagner, C. K. Kwok, E. Henke, S. Ergun, Generation of complex human organoid models including vascular networks by incorporation of mesodermal progenitor cells. *Sci. Rep.* **9**, 15663 (2019).
17. R. A. Wimmer, A. Leopoldi, M. Aichinger, D. Kerjaschki, J. M. Penninger, Generation of blood vessel organoids from human pluripotent stem cells. *Nat. Protoc.* **14**, 3082–3100 (2019).
18. R. A. Wimmer, A. Leopoldi, M. Aichinger, N. Wick, B. Hantusch, M. Novatchkova, J. Taubenschmid, M. Hammerle, C. Esk, J. A. Bagley, D. Lindenhofer, G. Chen, M. Boehm, C. A. Agu, F. Yang, B. Fu, J. Zuber, J. A. Knoblich, D. Kerjaschki, J. M. Penninger, Human blood vessel organoids as a model of diabetic vasculopathy. *Nature* **565**, 505–510 (2019).
19. X. Y. Sun, X. C. Ju, Y. Li, P. M. Zeng, J. Wu, Y. Y. Zhou, L. B. Shen, J. Dong, Y. J. Chen, Z. G. Luo, Generation of vascularized brain organoids to study neurovascular interactions. *eLife* **11**, e76707 (2022).
20. D. Kong, K. H. Park, D. H. Kim, N. G. Kim, S. E. Lee, N. Shin, M. G. Kook, Y. B. Kim, K. S. Kang, Cortical-blood vessel assembloids exhibit Alzheimer's disease phenotypes by activating glia after SARS-CoV-2 infection. *Cell Death Discov.* **9**, 32 (2023).
21. S. Inagaki, S. Nakamura, Y. Kuse, K. Aoshima, M. Funato, M. Shimazawa, H. Hara, Establishment of vascularized human retinal organoids from induced pluripotent stem cells. *Stem Cells* **43**, sxae093 (2025).
22. C. L. Bauwens, D. Toms, M. Ungrin, Aggregate size optimization in microwells for suspension-based cardiac differentiation of human pluripotent stem cells. *J. Vis. Exp.* **25**, 54308 (2016).
23. C. Quintard, E. Tubbs, G. Jonsson, J. Jiao, J. Wang, N. Werschler, C. Laporte, A. Pitaval, T. S. Bah, G. Pomeranz, C. Bissardon, J. Kaal, A. Leopoldi, D. A. Long, P. Blandin, J. L. Achard, C. Battail, A. Hagelkruys, F. Navarro, Y. Fouillet, J. M. Penninger, X. Gidrol, A microfluidic platform integrating functional vascularized organoids-on-chip. *Nat. Commun.* **15**, 1452 (2024).
24. E. Zudaire, L. Gambardella, C. Kurcz, S. Vermeren, A computational tool for quantitative analysis of vascular networks. *PLOS ONE* **6**, e27385 (2011).
25. H. Naderi-Meshkin, S. W. Wahyu, A. Yacoub, G. Carney, V. A. Cornelius, C. A. Nelson, S. Kelaini, C. Donaghy, P. D. Dunne, R. Amirkhah, A. Zampetaki, L. Zeng, A. W. Stitt, N. Lois, D. J. Grieve, A. Margariti, Unveiling impaired vascular function and cellular heterogeneity in diabetic donor-derived vascular organoids. *Stem Cells* **42**, 791–808 (2024).
26. F. Ginhoux, M. Greter, M. Leboeuf, S. Nandi, P. See, S. Gokhan, M. F. Mehler, S. J. Conway, L. G. Ng, E. R. Stanley, I. M. Samokhvalov, M. Merad, Fate mapping analysis reveals that adult microglia derive from primitive macrophages. *Science* **330**, 841–845 (2010).
27. Y. Zarb, S. Sridhar, S. Nassiri, S. G. Utz, J. Schaffenrath, U. Maheshwari, E. J. Rushing, K. Nilsson, M. Delorenzi, M. Colonna, M. Greter, A. Keller, Microglia control small vessel calcification via TREM2. *Sci. Adv.* **7**, eabc4898 (2021).
28. C. G. Fresta, A. Fidilio, G. Caruso, F. Caraci, F. J. Giblin, G. M. Leggio, S. Salomone, F. Drago, C. Bucolo, A new human blood-retinal barrier model based on endothelial cells, pericytes, and astrocytes. *Int. J. Mol. Sci.* **21**, 1636 (2020).
29. B. Cakir, Y. Xiang, Y. Tanaka, M. H. Kural, M. Parent, Y. J. Kang, K. Chapeton, B. Patterson, Y. Yuan, C. S. He, M. Raredon, J. Dengelegi, K. Y. Kim, P. Sun, M. Zhong, S. Lee, P. Patra, F. Hyder, L. E. Niklason, S. H. Lee, Y. S. Yoon, I. H. Park, Engineering of human brain organoids with a functional vascular-like system. *Nat. Methods* **16**, 1169–1175 (2019).
30. F. Bonanini, D. Kurek, S. Previdi, A. Nicolas, D. Hendriks, S. de Ruiter, M. Meyer, C. M. Clapes, R. Dinkelberg, S. B. Garcia, B. Kramer, T. Olivier, H. Hu, C. Lopez-Iglesias, F. Schavemaker, E. Walinga, D. Dutta, K. Queiroz, K. Domansky, B. Ronden, J. Joore, H. L. Lanz, P. J. Peters, S. J. Trietsch, H. Clevers, P. Vulto, In vitro grafting of hepatic spheroids and organoids on a microfluidic vascular bed. *Angiogenesis* **25**, 455–470 (2022).
31. S. Rajasekar, D. Lin, L. Abdul, A. Liu, A. Sotra, F. Zhang, B. Zhang, IFlowPlate-A customized 384-well plate for the culture of perfusable vascularized colon organoids. *Adv. Mater.* **32**, e2002974 (2020).
32. K. A. Homan, N. Gupta, K. T. Kroll, D. B. Kolesky, M. Skylar-Scott, T. Miyoshi, D. Mau, M. T. Valerius, T. Ferrante, J. V. Bonventre, J. A. Lewis, R. Morizane, Flow-enhanced vascularization and maturation of kidney organoids in vitro. *Nat. Methods* **16**, 255–262 (2019).
33. D. An, R. Pulford, W. H. Morgan, D. Y. Yu, C. Balaratnasingam, Associations between capillary diameter, capillary density, and microaneurysms in diabetic retinopathy: A high-resolution confocal microscopy study. *Transl. Vis. Sci. Technol.* **10**, 6 (2021).
34. L. Dao, Z. You, L. Lu, T. Xu, A. K. Sarkar, H. Zhu, M. Liu, R. Calandrelli, G. Yoshida, P. Lin, Y. Miao, S. Mierke, S. Kalva, H. Zhu, M. Gu, S. Vadivelu, S. Zhong, L. F. Huang, Z. Guo, Modeling blood-brain barrier formation and cerebral cavernous malformations in human PSC-derived organoids. *Cell Stem Cell* **31**, 818–833.e11 (2024).
35. Y. Ahn, J. H. An, H. J. Yang, D. G. Lee, J. Kim, H. Koh, Y. H. Park, B. S. Song, B. W. Sim, H. J. Lee, J. H. Lee, S. U. Kim, Human blood vessel organoids penetrate human cerebral organoids and form a vessel-like system. *Cells* **10**, 2036 (2021).
36. A. Armulik, G. Genové, C. Betsholtz, Pericytes: Developmental, physiological, and pathological perspectives, problems, and promises. *Dev. Cell* **21**, 193–215 (2011).
37. M. G. Kook, S. E. Lee, N. Shin, D. Kong, D. H. Kim, M. S. Kim, H. K. Kang, S. W. Choi, K. S. Kang, Generation of cortical brain organoid with vascularization by assembling with vascular spheroid. *Int J. Stem Cells* **15**, 85–94 (2022).
38. E. Carolina, Y. Kuse, A. Okumura, K. Aoshima, T. Tadokoro, S. Matsumoto, E. Kanai, T. Okumura, T. Kasai, S. Yamabe, Y. Nishikawa, K. Yamaguchi, Y. Furukawa, N. Tanimizu, H. Taniguchi, Generation of human iPSC-derived 3D bile duct within liver organoid by incorporating human iPSC-derived blood vessel. *Nat. Commun.* **15**, 7424 (2024).
39. M. O'Hara-Wright, A. Gonzalez-Cordero, Retinal organoids: A window into human retinal development. *Development* **147**, dev189746 (2020).
40. S. M. Silverman, W. T. Wong, Microglia in the retina: Roles in development, maturity, and disease. *Annu. Rev. Vis. Sci.* **4**, 45–77 (2018).
41. A. Buonfiglioli, R. Kubler, R. Missall, R. De Jong, S. Chan, V. Haage, S. Wendt, A. J. Lin, D. Mattei, M. Graziani, B. Latour, F. Gigase, R. Chiu, Y. Zhang, H. B. Nygaard, P. L. De Jager, L. D. De Witte, A microglia-containing cerebral organoid model to study early life immune challenges. *Brain Behav. Immun.* **123**, 1127–1146 (2025).
42. M. L. Gao, X. Zhang, F. Han, J. Xu, S. J. Yu, K. Jin, Z. B. Jin, Functional microglia derived from human pluripotent stem cells empower retinal organ. *Sci. China-Life Sci.* **65**, 1057–1071 (2022).

43. V. Chichagova, M. Georgiou, M. Carter, B. Dorgau, G. Hilgen, J. Collin, R. Queen, G. Chung, J. Ajeian, M. Moya-Molina, S. Kustermann, F. Pognan, P. Hewitt, M. Schmitt, E. Sernagor, L. Armstrong, M. Lako, Incorporating microglia-like cells in human induced pluripotent stem cell-derived retinal organoids. *J. Cell. Mol. Med.* **27**, 435–445 (2023).
44. S. Sabate-Soler, S. L. Nickels, C. Saraiva, E. Berger, U. Dubonyte, K. Barmpa, Y. J. Lan, T. Kouno, J. Jarazo, G. Robertson, J. Sharif, H. Koseki, C. Thome, J. W. Shin, S. A. Cowley, J. C. Schwamborn, Microglia integration into human midbrain organoids leads to increased neuronal maturation and functionality. *Glia* **70**, 1267–1288 (2022).
45. K. Bora, N. Kushwah, M. Maurya, M. C. Pavlovich, Z. Wang, J. Chen, Assessment of inner blood-retinal barrier: Animal models and methods. *Cells* **12**, 2443 (2023).
46. M. Furuse, H. Sasaki, K. Fujimoto, S. Tsukita, A single gene product, claudin-1 or -2, reconstitutes tight junction strands and recruits occludin in fibroblasts. *J. Cell Biol.* **143**, 391–401 (1998).
47. E. H. Shue, E. B. Carson-Walter, Y. Liu, B. N. Winans, Z. S. Ali, J. Chen, K. A. Walter, Plasmalemmal vesicle associated protein-1 (PV-1) is a marker of blood-brain barrier disruption in rodent models. *BMC Neurosci.* **9**, 29 (2008).
48. N. J. Abbott, L. Rönnbäck, E. Hansson, Astrocyte-endothelial interactions at the blood-brain barrier. *Nat. Rev. Neurosci.* **7**, 41–53 (2006).
49. X. Sun, Z. Cui, Y. Liang, C. Duan, H. F. Chan, S. Mao, J. Gu, C. Ding, X. Yang, Q. Wang, S. Tang, J. Chen, One-stop assembly of adherent 3D retinal organoids from hiPSCs based on 3D-printed derived PDMS microwell platform. *Biofabrication* **15**, 035005 (2023).
50. X. Zhong, C. Gutierrez, T. Xue, C. Hampton, M. N. Vergara, L. H. Cao, A. Peters, T. S. Park, E. T. Zambidis, J. S. Meyer, D. M. Gamm, K. W. Yau, M. V. Canto-Soler, Generation of three-dimensional retinal tissue with functional photoreceptors from human iPSCs. *Nat. Commun.* **5**, 4047 (2014).

Acknowledgments

Funding: This study was supported by the National Natural Science Foundation of China (NSFC-RGC: N_CUHK432/20, 32061160469), the Natural Science Foundation of Hunan Province, China (2024JJ6001), the China Postdoctoral Science Foundation (2024M760003), and the Science Research Grant of Aier Eye Institute, China (grant no. AEI202302JC02). **Author contributions:** Conceptualization: J.C., H.F.C., and H.C. Methodology: J.C., H.F.C., H.C., Yuqin Liang, and X.S. Investigation: J.C., H.F.C., H.C., Yuqin Liang, and X.S. Data curation: J.C., H.F.C., and H.C.. Validation: H.C., Yuqin Liang, X.S., W.X., T.Y., Yuan Liang, W.W., and X.L. Formal analysis: H.C., Yuqin Liang, X.S., and X.Y. Software: H.C., Yuqin Liang, and X.S. Resources: J.C., H.F.C., J.Z., and L.C. Visualization: J.C., H.F.C., H.C., Yuqin Liang, and X.S. Supervision: J.C. and H.F.C. Project administration: J.C. and H.F.C. Writing–original draft: J.C., H.C., Yuqin Liang, and X.S. Writing–review and editing: J.C. and H.F.C. Funding acquisition: J.C., H.C., Yuqin Liang, X.S., and J.G. **Competing interests:** The authors declare that they have no competing interests. **Data and materials availability:** All data needed to evaluate the conclusions in the paper are present in the paper and/or the Supplementary Materials.

Submitted 10 May 2025
Accepted 11 September 2025
Published 10 October 2025
10.1126/sciadv.ady6410